J. Fluid Mech. (1998), *vol.* 359, *pp.* 217–237. Printed in the United Kingdom

Torsional flow: effect of second normal stress difference on elastic instability in a finite domain

By AARON AVAGLIANO AND NHAN PHAN-THIEN

Department of Mechanical & Mechatronic Engineering,
The University of Sydney, NSW 2006, Australia

(Received 24 April 1997 and in revised form 25 October 1997)

A rotational shear flow is examined in the bounded parallel-plate geometry for a four-constant Oldroyd-type fluid which has a constant viscosity, and constant first and second normal stress coefficients. A new type of Galerkin spectral technique is introduced to solve the resulting two-dimensional stiff boundary value problem. We show that even a small second normal stress difference can lead to a significant increase (nearly 100 %) in the stability of the base torsional flow. Beyond a critical Deborah number the secondary flow, in the form of travelling waves, appears to be confined between two critical radii, in qualitative agreement with the experimental results of Byars *et al.* (1994). The mechanism behind this instability is investigated for dilute polymer solutions.

1. Introduction

Comparison of recent theoretical and experimental results in the area of viscoelastic flows with curved streamlines has shown that the Oldroyd-B model does not accurately describe the transition to secondary flow of a Boger fluid when the base flow becomes unstable.

The key ingredients in the stability analysis of parallel-plate flows appear to be that above a critical rotation rate of the upper (or lower) plate, the base torsional solution becomes unstable to infinitesimal disturbances, and that the form of the resulting flow in the region of linear instability is that of a travelling wave that appears to be confined between two critical radii (a Hopf bifurcation leading to a time-dependent secondary flow). This travelling wave takes the form of a spiral vortex (three-dimensional non-axisymmetric disturbances) or concentric toroidal roll cells (two-dimensional axisymmetric disturbances). The critical mode of the disturbance is highly dependent on both the material properties and the flow geometry (Byars *et al.* 1994).

Avagliano & Phan-Thien (1996) showed that the consideration of a finite geometry (as opposed to one extending infinitely in the radial direction) leads to a significant improvement in this correlation. Taking into account all possible axisymmetric infinitesimal disturbances, they show that beyond a critical radius the amplitude of the secondary flow changes by approximately three orders of magnitude. Hence the secondary flow would appear only within a bounded region, rather than the entire fluid domain. However, the model is still rather poor at predicting both the critical rotation rate and the location of the resulting secondary flow. The predicted critical rotation rate was much lower than the corresponding experimental values unless a more suitable choice of relaxation time is made, for example that of Öztekin & Brown (1993). Also, the critical radii between which toroidal travelling waves could

be seen were much closer to the outer edge of the discs than the experiments of Byars *et al.* (1994) have shown to be the case.

The difference between theory and experiment has mostly been attributed to the fact that many, but not all, of the experimental fluids exhibit shear thinning, particularly of the first normal stress coefficient Ψ_1, over the relevant range of shear rates. Successful attempts have been made to incorporate shear thinning in the theoretical models applied to the parallel-plate geometry. For example, Byars *et al.* (1994) employed the Chilcott–Rallison model to obtain a better approximation to the critical radii than the overprediction offered by the Oldroyd-B model. Another limiting factor of theoretical analyses to date has been the use of a single relaxation time in the constitutive model of the extra stress $\boldsymbol{S}_*$. Small-strain and small-amplitude oscillatory tests with these Boger fluids by Quinzani *et al.* (1990) have shown that a spectrum of relaxation times is necessary to adequately model the relaxation modulus in order to predict rheological properties like dynamic viscosity and storage modulus. Their steady shear flow results show that Ψ_1 exhibits shear-thinning behaviour with increasing shear rate, but also plateaus at intermediate shear rates, indicating that a constitutive model that is nonlinear in stress may be necessary to capture the rheology of these fluids at the intermediate shear rates at which rotational instability occurs. Olagunju (1994) used a perturbation scheme to show that the effect of a free surface on stability is minimal, since it is perturbed by only a small amount due to secondary flows. A recent discussion of these difficulties as well as a review of elastic instabilities arising from other viscometric flows is available in Shaqfeh (1996).

Since Boger fluids have been used in much of the experimental work (these fluids have negligible second normal stress coefficient Ψ_2), the importance of Ψ_2 has not been taken into account. Experimental measurement of the stress ratio Ψ_2/Ψ_1 has proven exceedingly difficult for these fluids. Magda *et al.* (1991) have measured this ratio as $\Psi_2/\Psi_1 = -0.01 \pm 0.01$, indicating that if Ψ_2 were non-zero, then a more accurate measurement was beyond the capability of the experimental apparatus employed. It has been demonstrated theoretically, at least in a semi-infinite geometry, that a negative second normal stress coefficient leads to a stabilization of the base flow and consequently secondary flow sets in at a higher critical rotation rate (Phan-Thien & Huilgol 1985). We show in this paper that the introduction of even a small Ψ_2 ($\sim -0.5\%\,\Psi_1$) leads to a significant increase in the stability of the base flow (approximately a 100% increase in critical rotation rate for small aspect ratio). The critical radii of the disturbance flow are also significantly reduced, allowing a much better correlation with the experimental results of Byars *et al.* (1994).

2. Flow geometry and governing equations

The parallel-plate geometry is modelled identically with the finite domain approach used in Avagliano & Phan-Thien (1996). Two flat circular plates of radius R are held horizontally a distance h apart as shown in figure 1, with a common vertical axis through their centres. The fluid is contained between the plates by a frictionless bounding surface at $r_* = R$. With the bottom plate held fixed, the top plate is set spinning at an angular velocity ω.

The governing field equations are

$$\rho \frac{\mathrm{D}\boldsymbol{v}_*}{\mathrm{D}t} = -\nabla_* P_* + \nabla_* \cdot \boldsymbol{S}_* , \qquad \nabla_* \cdot \boldsymbol{v}_* = 0, \tag{2.1}$$

where ρ is the fluid density, $\mathrm{D}/\mathrm{D}t$ the material time derivative, P_* the pressure field,

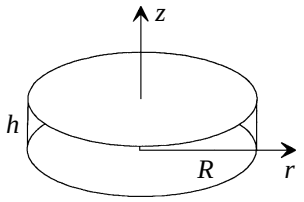

FIGURE 1. Flow geometry.

and $\boldsymbol{S}_*$ and $\boldsymbol{v}_*$ the extra stress and the velocity fields, respectively. For an Oldroyd-type constitutive equation, $\boldsymbol{S}_*$ is given by $\boldsymbol{S}_* = \boldsymbol{\tau}_{s*} + \boldsymbol{\tau}_{p*}$, a sum of solvent and polymeric contributions to the total stress. The solvent contribution is simply the Newtonian stress term $\boldsymbol{\tau}_{s*} = 2\eta_s \boldsymbol{D}_*$, while for the polymeric stress, we consider an adaptation to the Oldroyd-eight-constant model, adopted in Phan-Thien & Huilgol (1985) to examine the effect of Ψ_2 on torsional flow stability. The polymeric stress for this model is determined from a quasi-linear partial differential equation which is linear in $\boldsymbol{\tau}_{p*}$:

$$\boldsymbol{\tau}_{p*} + \lambda \left\{ \frac{\partial \boldsymbol{\tau}_{p*}}{\partial t} + \boldsymbol{v}_* \cdot \nabla \boldsymbol{\tau}_{p*} - \boldsymbol{L}_* \tau_{p*} - \boldsymbol{\tau}_{p*} \boldsymbol{L}_*^T \right\} = 2\eta_p \left\{ \boldsymbol{D}_* - \mu\lambda \boldsymbol{D}_*^2 + \tfrac{1}{2}\mu\lambda \,\mathrm{tr}\left(\boldsymbol{D}_*^2\right) \boldsymbol{I} \right\}. \quad (2.2)$$

Here we have λ as the sole relaxation time, $\boldsymbol{L}_* = (\nabla_* \boldsymbol{v}_*)^T$ is the velocity gradient tensor, with $\boldsymbol{D}_*$ as its symmetric part, and the total viscosity $\eta = \eta_s + \eta_p$. The importance of the extra parameter μ is revealed when considering a simple shear flow at constant shear rate, where it can be found that the ratio of the second to the first normal stress difference is given by

$$\frac{\Psi_2}{\Psi_1} = -\frac{\mu}{4}, \quad (2.3)$$

and consequently the addition of a second normal stress coefficient to the Oldroyd-B model ($\mu = 0$) can be accomplished with positive or negative values of μ. The second normal stress coefficient in most polymer *melts* is negative, and is of the order 10 % of the first normal stress coefficient. For these fluids, μ is of order unity. To compare the theoretical predictions to the results of McKinley *et al.* (1991) and Byars *et al.* (1994), a representative value of $\mu = 0.025$ was chosen. This is within the range determined experimentally for these fluids by Magda *et al.* (1991). Although four parameters are employed in this model, we mention here that this is not the same constitutive equation as the more widely known Oldroyd-four-constant model which has been discussed in Bird, Armstrong & Hassager (1987).

For cylindrical polar coordinates (r_*, θ, z_*) we non-dimensionalize the variables as

$$\left.\begin{gathered} z = \frac{z_*}{h}, \quad r = \frac{r_*}{R}, \quad t = \omega t_*, \quad v_\theta = \frac{v_{\theta*}}{\omega R}, \quad v_r = \frac{v_{r*}}{\omega R}, \quad v_z = \frac{v_{z*}}{\omega h}, \\ De = \lambda\omega, \quad \varepsilon = \frac{h}{R}, \quad Re = \frac{\rho\omega h R}{\eta}, \quad \beta = \frac{\eta_p}{\eta}, \\ P = \varepsilon^2 \frac{P_*}{\eta\omega}, \quad \tau_{zz} = \frac{\tau_{pzz*}}{\eta\omega}, \quad \tau_{rz} = \varepsilon \frac{\tau_{prz*}}{\eta\omega}, \quad \tau_{rr} = \varepsilon^2 \frac{\tau_{prr*}}{\eta\omega}, \\ \tau_{\theta\theta} = \varepsilon^2 \frac{\tau_{p\theta\theta*}}{\eta\omega}, \quad \tau_{r\theta} = \varepsilon^2 \frac{\tau_{pr\theta*}}{\eta\omega}, \quad \tau_{\theta z} = \varepsilon \frac{\tau_{p\theta z*}}{\eta\omega}. \end{gathered}\right\} \quad (2.4)$$

Here De, the Deborah number, is a dimensionless rotation rate, being the ratio of the fluid relaxation time to the characteristic time scale. A Weissenberg number, or

dimensionless shear rate can be calculated from the rim shear rate as $Wi = De/\varepsilon$. Re is the Reynolds number, β is the retardation parameter ($\beta = 0$ gives the Newtonian case), and ε is the aspect ratio of the discs.

2.1. *Boundary conditions*

The no-slip boundary conditions on the upper and lower plates require that

$$\left.\begin{array}{c} v_r = v_z = v_\theta = 0 \quad \text{at} \quad z = 0, \\ v_r = v_z = 0, \quad v_\theta = r \quad \text{at} \quad z = 1. \end{array}\right\} \tag{2.5}$$

Symmetry conditions at the centreline dictate a zero radial and azimuthal velocity, as well as zero shear stress there, i.e.

$$v_r = v_\theta = 0, \quad \tau_{r\theta} = \tau_{rz} = 0 \quad \text{at} \quad r = 0. \tag{2.6}$$

On the frictionless outer shell we have no flow through the boundary ($\boldsymbol{v} \cdot \boldsymbol{n} = 0$, $\boldsymbol{n} = (1, 0, 0)$), and the traction only acts in a direction normal to the boundary ($\boldsymbol{\tau} \cdot \boldsymbol{n} - \boldsymbol{\tau} : \boldsymbol{nnn} = \boldsymbol{0}$), i.e.

$$v_r = 0, \quad \tau_{r\theta} = \tau_{rz} = 0 \quad \text{at} \quad r = 1. \tag{2.7}$$

2.2. *Base solution*

We assume an inertialess flow regime to determine the secondary flow instabilities due solely to the fluid elasticity. The governing equations may be written as

$$-\frac{\partial P}{\partial r} + \frac{1}{r}\frac{\partial}{\partial r}(r\tau_{rr}) + \frac{\partial \tau_{rz}}{\partial z} - \frac{\tau_{\theta\theta}}{r} + (1-\beta)\left[\varepsilon^2 \frac{\partial}{\partial r}\left(\frac{1}{r}\frac{\partial}{\partial r}(rv_r)\right) + \frac{\partial^2 v_r}{\partial z^2}\right] = 0, \tag{2.8}$$

$$\frac{1}{r^2}\frac{\partial}{\partial r}\left(r^2\tau_{r\theta}\right) + \frac{\partial \tau_{\theta z}}{\partial z} + (1-\beta)\left[\varepsilon^2 \frac{\partial}{\partial r}\left(\frac{1}{r}\frac{\partial}{\partial r}(rv_\theta)\right) + \frac{\partial^2 v_\theta}{\partial z^2}\right] = 0, \tag{2.9}$$

$$-\frac{\partial P}{\partial z} + \varepsilon^2\left\{\frac{1}{r}\frac{\partial}{\partial r}(r\tau_{rz}) + \frac{\partial \tau_{zz}}{\partial z}\right\} + (1-\beta)\left[\varepsilon^4 \frac{1}{r}\frac{\partial}{\partial r}\left(r\frac{\partial v_z}{\partial r}\right) + \varepsilon^2 \frac{\partial^2 v_z}{\partial z^2}\right] = 0, \tag{2.10}$$

$$\frac{1}{r}\frac{\partial}{\partial r}(rv_r) + \frac{\partial v_z}{\partial z} = 0, \tag{2.11}$$

$$\mathfrak{I}(\boldsymbol{\tau})_{zz} = \beta\left\{2\frac{\partial v_z}{\partial z} + \mu De\left[\left(\frac{\partial v_r}{\partial r}\right)^2 + \left(\frac{v_r}{r}\right)^2 - \left(\frac{\partial v_z}{\partial z}\right)^2 + \frac{1}{2}\left(r\frac{\partial}{\partial r}\left(\frac{v_\theta}{r}\right)\right)^2\right]\right\}, \tag{2.12}$$

$$\mathfrak{I}(\boldsymbol{\tau})_{\theta z} = \beta\left\{\frac{\partial v_\theta}{\partial z} - \mu De\left[\frac{1}{2}r\frac{\partial}{\partial r}\left(\frac{v_\theta}{r}\right)\left(\frac{\partial v_r}{\partial z} + \varepsilon^2\frac{\partial v_z}{\partial r}\right) + \frac{\partial v_\theta}{\partial z}\left(\frac{\partial v_z}{\partial z} + \frac{v_r}{r}\right)\right]\right\}, \tag{2.13}$$

$$\mathfrak{I}(\boldsymbol{\tau})_{rz} = \beta\left\{\frac{\partial v_r}{\partial z} + \varepsilon^2\frac{\partial v_z}{\partial r} - \mu De\left[\left(\frac{\partial v_z}{\partial z} + \frac{\partial v_r}{\partial r}\right)\left(\frac{\partial v_r}{\partial z} + \varepsilon^2\frac{\partial v_z}{\partial r}\right) + \frac{1}{2}r\frac{\partial v_\theta}{\partial z}\frac{\partial}{\partial r}\left(\frac{v_\theta}{r}\right)\right]\right\}, \tag{2.14}$$

$$\mathfrak{I}(\boldsymbol{\tau})_{r\theta} = \beta\left\{\varepsilon^2 r\frac{\partial}{\partial r}\left(\frac{v_\theta}{r}\right) - \mu De\left[\varepsilon^2 r\frac{\partial}{\partial r}\left(\frac{v_\theta}{r}\right)\left(\frac{\partial v_r}{\partial r}+\frac{v_r}{r}\right)+\frac{1}{2}\frac{\partial v_\theta}{\partial z}\left(\frac{\partial v_r}{\partial z}+\varepsilon^2\frac{\partial v_z}{\partial r}\right)\right]\right\}, \tag{2.15}$$

$$\mathfrak{I}(\boldsymbol{\tau})_{\theta\theta} = \beta\left\{2\varepsilon^2\frac{v_r}{r}+\mu De\varepsilon^2\left[\left(\frac{\partial v_r}{\partial r}\right)^2-\left(\frac{v_r}{r}\right)^2+\left(\frac{\partial v_z}{\partial z}\right)^2+\frac{1}{2\varepsilon^2}\left(\frac{\partial v_r}{\partial z}+\varepsilon^2\frac{\partial v_z}{\partial r}\right)^2\right]\right\}, \tag{2.16}$$

$$\mathfrak{I}(\boldsymbol{\tau})_{rr} = \beta\left\{2\varepsilon^2\frac{\partial v_r}{\partial r}+\mu De\varepsilon^2\left[\left(\frac{v_r}{r}\right)^2+\left(\frac{\partial v_z}{\partial z}\right)^2+\frac{1}{2\varepsilon^2}\left(\frac{\partial v_\theta}{\partial z}\right)^2-\left(\frac{\partial v_r}{\partial r}\right)^2\right]\right\}, \tag{2.17}$$

where $\mathfrak{I}(\boldsymbol{\tau})$ is the tensor operator on the right-hand side of (2.2).

The base solution for this problem is the viscometric solution

$$\left.\begin{aligned} v_r = v_z = 0, \quad v_\theta = rz, \quad P = P_{const} + \left(\tfrac{3}{4}\mu - 1\right) De\beta r^2, \\ \tau_{r\theta} = \tau_{rz} = \tau_{zz} = 0, \quad \tau_{\theta z} = \beta r, \quad \tau_{\theta\theta} = 2De\beta r^2,\ \tau_{rr} = \tfrac{1}{2}\mu De\beta r^2. \end{aligned}\right\} \tag{2.18}$$

3. Linear stability analysis

In order to examine the stability of (2.18) to infinitesimal axisymmetric disturbances, we assume the functional form

$$\left.\begin{aligned} \boldsymbol{v} &= \boldsymbol{v}_o + \delta\,\mathrm{Re}\left[\mathrm{e}^{(\sigma/De)t}\,\boldsymbol{u}(r,z)\right], \\ \boldsymbol{\tau} &= \boldsymbol{\tau}_o + \delta\,\mathrm{Re}\left[\mathrm{e}^{(\sigma/De)t}\,\boldsymbol{\sigma}(r,z)\right], \\ P &= P_o + \delta\,\mathrm{Re}\left[\mathrm{e}^{(\sigma/De)t}p(r,z)\right], \end{aligned}\right\} \tag{3.1}$$

where $\mathrm{Re}[\cdot]$ represents the real part, $\boldsymbol{v}_o$, $\boldsymbol{\tau}_o$, and P_o are the base solution, and σ is the critical parameter representing the growth rate of the infinitesimal disturbance. If $\mathrm{Re}(\sigma) < 0$, the base solution is stable, $\mathrm{Re}(\sigma) > 0$ implies the solution is linearly unstable in this region of $(De, \varepsilon, \beta, \mu)$-space, and $\mathrm{Re}(\sigma) = 0$ supplies neutral stability curves between the material and geometric parameters.

Substitution of (3.1) into the constitutive equations yields the perturbed stress field as a function of the perturbed velocities. A stream function is introduced to eliminate the mass conservation equation, and the pressure is eliminated from the momentum equations as in Avagliano & Phan-Thien (1996). The resulting pair of governing equations is of the form

$$\begin{aligned} &(1+\sigma)\ [1+\sigma(1-\beta)]\left\{\varepsilon^2\frac{\partial}{\partial r}\left(\frac{1}{r}\frac{\partial}{\partial r}(ru_\theta)\right)+\frac{\partial^2 u_\theta}{\partial z^2}\right\} \\ &\quad +De\beta\left\{\frac{\partial^3\varphi}{\partial z^2\partial r}-\frac{2(2+\sigma)}{r}\frac{\partial^2\varphi}{\partial z^2}+\varepsilon^2\frac{\partial}{\partial r}\left(\frac{1}{r}\frac{\partial}{\partial r}\left(r\frac{\partial\varphi}{\partial r}\right)\right)\right\} \\ &\quad -\frac{\mu De\beta}{2}\left\{-De\sigma\frac{1}{r^2}\frac{\partial}{\partial r}\left(r^5\frac{\partial}{\partial r}\left(\frac{u_\theta}{r}\right)\right)-De^2\frac{1}{r^2}\frac{\partial}{\partial r}\left(r^5\frac{\partial}{\partial r}\left(\frac{1}{r}\frac{\partial\varphi}{\partial r}\right)\right)\right. \\ &\quad \left.+(1+\sigma)\left[\frac{\partial^3\varphi}{\partial z^2\partial r}-\frac{4}{r}\frac{\partial^2\varphi}{\partial z^2}+\varepsilon^2\frac{\partial}{\partial r}\left(\frac{1}{r}\frac{\partial}{\partial r}\left(r\frac{\partial\varphi}{\partial r}\right)\right)\right]\right\}=0, \end{aligned} \tag{3.2}$$

$$2De\beta\ (1+\sigma)(2+\sigma)\frac{\partial^2 u_\theta}{\partial z^2}+2De^2\beta(3+\sigma)\frac{\partial^3\varphi}{\partial r\partial z^2}+(1+\sigma)^2[1+\sigma(1-\beta)]$$
$$\times\left\{\frac{1}{r}\frac{\partial^4\varphi}{\partial z^4}+2\varepsilon^2\frac{\partial}{\partial r}\left(\frac{1}{r}\frac{\partial^3\varphi}{\partial r\partial z^2}\right)+\varepsilon^4\frac{\partial}{\partial r}\left(\frac{1}{r}\frac{\partial}{\partial r}\left(r\frac{\partial}{\partial r}\left(\frac{1}{r}\frac{\partial\varphi}{\partial r}\right)\right)\right)\right\}$$
$$-\frac{\mu De\beta}{2}\left\{(1+\sigma)^2\left[\frac{1}{r^4}\frac{\partial}{\partial r}\left(r^5\frac{\partial^2 u_\theta}{\partial z^2}\right)+\varepsilon^2\frac{\partial}{\partial r}\left(r\frac{\partial}{\partial r}\left(\frac{1}{r}\frac{\partial}{\partial r}(ru_\theta)\right)\right)\right.\right.$$
$$\left.\left.-De\left(\varepsilon^2\frac{\partial}{\partial r}\left(r\frac{\partial}{\partial r}\left(\frac{1}{r}\frac{\partial}{\partial r}\left(r\frac{\partial\varphi}{\partial r}\right)\right)\right)+r^2\frac{\partial}{\partial r}\left(\frac{1}{r^3}\frac{\partial}{\partial r}\left(r^2\frac{\partial^2\varphi}{\partial z^2}\right)\right)\right)\right]$$
$$+4De(1+\sigma)\left[\frac{\partial^3\varphi}{\partial r\partial z^2}-\frac{1}{r}\frac{\partial^2\varphi}{\partial z^2}\right]\right\}=0, \tag{3.3}$$

with

$$u_r=-\frac{1}{r}\frac{\partial\varphi}{\partial z},\quad u_z=\frac{1}{r}\frac{\partial\varphi}{\partial r}. \tag{3.4}$$

Examination of (3.3) reveals that the differential equation is third order in r for u_θ, whilst there are only two radial boundary conditions for this variable. Two methods were developed for overcoming this problem. The first method involves eliminating the term involving $\partial^3 u_\theta/\partial r^3$ between equations (3.2) and (3.3) to obtain a third equation that can be solved in conjunction with (3.2). No extra boundary conditions need to be supplied with this method, and it may be hoped that, due to removal of the higher-order derivative, the numerical scheme employed will converge more quickly. The drawback is that a term involving σ^5 is created and this leads to significantly larger matrix size in the matrix eigenvalue problem resulting from the numerical scheme.

The second, preferred method involves using pole conditions to manufacture an extra boundary condition. This will be a natural boundary condition and, while not altering the eventual solution, a correct choice of pole condition will lead to an improvement in the rate of convergence of the numerical solution to (3.2)–(3.3). A discussion of pole conditions and their applicability can be found in Gottleib & Orszag (1977).

4. Numerical schemes

The boundary conditions are appropriately determined already, due to the fact that the two centreline conditions $u_\theta=0,\quad \sigma_{r\theta}=0$ at $r=0$ are identical, and do not lead to an overdetermined system. Expressed in terms of the stream function, the stress and velocity boundary conditions at $r=0,1$ become

$$\frac{1}{r}\frac{\partial\varphi}{\partial z}=\frac{\partial}{\partial r}\left(\frac{1}{r}\frac{\partial\varphi}{\partial r}\right)=r\frac{\partial}{\partial r}\left(\frac{u_\theta}{r}\right)=0.$$

The pole condition is derived from (3.2) in the limit $r\to 0$:

$$\frac{\partial}{\partial r}\left(\frac{1}{r}\frac{\partial}{\partial r}(ru_\theta)\right)=0\quad\text{at}\quad r=0.$$

The coupled partial differential equations are solved via a Galerkin spectral technique similar to that discussed in Avagliano & Phan-Thien (1996).

The radial coordinate is stretched by the transformation $x = 2r - 1$ to the domain $[-1, 1]$, so that Chebyshev polynomials can be employed to resolve the solution in the radial direction. The periodic nature of the boundary conditions in the vertical direction allows the use of trigonometric polynomials in the axial coordinate. The highest-order derivatives of each dependent variable are expressed in terms of this infinite double sum in the manner of Zebib (1984). This ensures that all of the terms in (3.2)–(3.3) are represented by a complete set of linearly independent functions:

$$\frac{\partial^5 u_\theta}{\partial x^3 \partial z^2} = \sum_{i=0}^{\infty}\sum_{j=0}^{\infty} \alpha_{ij} T_i(x) \cos(j\pi z), \tag{4.1}$$

$$\frac{\partial^8 \varphi}{\partial x^4 \partial z^4} = \sum_{i=0}^{\infty}\sum_{j=0}^{\infty} \beta_{ij} T_i(x) \cos(j\pi z). \tag{4.2}$$

The appropriate boundary conditions are easily implemented by integrating the above equations to obtain a set of trial functions for each dependent variable as

$$u_\theta = \sum_{n=1}^{\infty}\sum_{i=1}^{n} a_{(n(n-1)/2+i-1)} \Lambda_{n-i+1}(x) \Pi_i(z), \tag{4.3}$$

$$\varphi = \sum_{n=1}^{\infty}\sum_{i=1}^{n} b_{(n(n-1)/2+i-1)} \Psi_{n-i+1}(x) \Phi_i(z), \tag{4.4}$$

where Λ, Π, Ψ, and Φ satisfy all of the imposed boundary conditions.

4.1. *Petrov–Galerkin scheme*

Considering the set of coupled partial differential equations as being in the form $\Im_1(u_\theta, \varphi;\ De, \sigma, \beta, \varepsilon, \mu) = 0$, $\Im_2(u_\theta, \varphi; De, \sigma, \beta, \varepsilon, \mu) = 0$, respectively, where $\Im_1$ and $\Im_2$ are linear partial differential operators, and observing that the Nth partial sums of (4.3) and (4.4),

$$u_{\theta N} = \sum_{n=1}^{N}\sum_{i=1}^{n} a_{(n(n-1)/2+i-1)} \Lambda_{n-i+1}(x) \Pi_i(z), \tag{4.5}$$

$$\varphi_N = \sum_{n=1}^{N}\sum_{i=1}^{n} b_{(n(n-1)/2+i-1)} \Psi_{n-i+1}(x) \Phi_i(z), \tag{4.6}$$

each contain $N(N+1)/2$ linearly independent terms, we can now introduce the Petrov–Galerkin scheme by forming the residuals of $\Im_1$ and $\Im_2$, and taking appropriate inner products, i.e.

$$\langle \Im_1(u_{\theta N}, \varphi_N), u_{\theta mk} \rangle = 0, \quad u_{\theta mk} = \Lambda_{m-k+1} \Pi_k,$$

$$\langle \Im_2(u_{\theta N}, \varphi_N), \varphi_{mk} \rangle = 0, \quad \varphi_{mk} = \Psi_{m-k+1} \Phi_k\ ,\ m = 1, \ldots, N,\ k = 1, \ldots, m,$$

with

$$\langle u(x,z), v(x,z) \rangle = \iint_S w(x)\, u(x,z)\, v(x,z)\, \mathrm{d}S = \int_0^1 \int_{-1}^1 \frac{1}{(1-x^2)^{1/2}} uv\ \mathrm{d}x\ \mathrm{d}z. \tag{4.7}$$

N	Matrix dimension	De_c ($\mu = 0$)	De_c ($\mu = 0.025$)
11	396	1.671	2.771
12	468	—	2.667
13	546	1.663	2.648
14	630	1.661	2.708
15	720	1.661	2.678
16	816	—	2.648
17	918	—	2.637

TABLE 1. The slow convergence of the Petrov–Galerkin scheme.

4.1.1. *Associated matrix eigenvalue problem*

The Petrov–Galerkin scheme defined in (4.7) yields a third-order polynomial eigenvalue problem for the coupled system

$$\left[\sigma^3 \boldsymbol{B}_3 + \sigma^2 \boldsymbol{B}_2 + \sigma \boldsymbol{B}_1 + \boldsymbol{A}\right] \boldsymbol{v} = 0, \tag{4.8}$$

where $\boldsymbol{A}$, $\boldsymbol{B}_1$, $\boldsymbol{B}_2$, $\boldsymbol{B}_3$ are all square matrices of size $N_T = N(N+1)$. They are also functions of the parameters De, β, ε, and μ. The coefficients of the trial functions are stored in $\boldsymbol{v}$, where

$$\boldsymbol{v} = \left(a_0, a_1, .., a_{N_T/2-1}, b_0, b_1, .., b_{N_T/2-1}\right)^T. \tag{4.9}$$

In general $\boldsymbol{B}_3$ will be a singular matrix with $N_T/2$ zero rows, whilst $\boldsymbol{A}$ is non-singular. It thus becomes necessary to remove the infinite eigenvalues arising from the singularity of $\boldsymbol{B}_3$. They are mapped to 0 using the transformation $v = 1/\sigma$. The infinite eigenvalues arise as a consequence of the discretization, and are not solutions to the actual problem. Since their exact number is known $(N_T/2)$, the resulting eigenvalues can be discounted when determining the critical modes. Note that this transformation preserves the positions of all eigenvalues with respect to the real half-planes. Introducing $\boldsymbol{w} = (v^2\boldsymbol{v}, v\boldsymbol{v}, \boldsymbol{v})^T$, we have the generalized eigenvalue problem

$$\begin{pmatrix} -\boldsymbol{B}_1 & -\boldsymbol{B}_2 & -\boldsymbol{B}_3 \\ \boldsymbol{I} & 0 & 0 \\ 0 & \boldsymbol{I} & 0 \end{pmatrix} \boldsymbol{w} = v \begin{pmatrix} \boldsymbol{A} & 0 & 0 \\ 0 & \boldsymbol{I} & 0 \\ 0 & 0 & \boldsymbol{I} \end{pmatrix} \boldsymbol{w}. \tag{4.10}$$

For fixed values of β, ε, and μ the critical Deborah number De_c of the torsional flow can be determined from examination of the eigenvalues of (4.10). When $\mathrm{Re}(v) < 0$ the viscometric solution is stable to infinitesimal disturbances, whilst $\mathrm{Re}(v) > 0$ implies the solution will be unstable and criticality occurs when $\mathrm{Re}(v) = 0$ (this is valid since all the bifurcations are Hopf bifurcations, i.e. the critical σ is complex).

4.1.2. *Convergence of the Petrov–Galerkin scheme*

The convergence of the scheme is quite poor. For $\mu = 0$ four significant figure accuracy was obtained at $N = 15$ (matrix size 720×720). However for $\mu = 0.025$ only one significant figure was possible at $N = 17$ (matrix size 918×918) as the scheme oscillated between 2.6 and 2.7 rather than converging. Results for the Oldroyd-B model and for a small Ψ_2 are summarized in table 1. Here we have chosen $\beta = 0.41$ (the same value as used in the flow visualization experiments of McKinley *et al.* 1991 and Byars *et al.* 1994) and $\varepsilon = 0.1$.

The cause of the slow convergence can be understood in a general sense upon examination of the functional form of the disturbance, or the actual nature and

location of the toroidal roll cells that constitute the secondary flow. From figure 6 we observe that the large-amplitude roll cells have moved toward the centre of the discs at $\mu = 0.025$ rather than remaining near the outer edge as they were for the Oldroyd-B model. Mathematically this means that the Chebyshev polynomials employed in the numerical scheme will require a greater number of modes in the radial direction to converge (e.g. Peyret 1989).

4.2. *Alternative Galerkin scheme*

Owing to the differing orders of magnitude of the two length scales h and R in this problem, a feature of stiff boundary value problems in general, and in particular the difficulty in resolving the solution in the radial direction, the standard Galerkin method seems an inefficient solution method. This is due to the fact that whilst a high number of Chebyshev modes are required for convergence, the introduction of each new mode necessitates the introduction of a higher-order Fourier mode in the vertical direction and also all of the interactions of the modes of this order.

The order of approximation of the dependent variables in the standard Galerkin scheme (4.5)–(4.6) is determined by the single integer parameter N. This new method introduces three integer parameters to determine which of the terms in (4.3)–(4.4) are included in each successive approximation to the spectral solution. Let N_r be the highest-order mode in the radial direction, N_z be the highest-order mode in the vertical direction, and N_i the number of modes to be included of order N_r and assume for simplicity that $N_i < N_z$ (usually $N_i < 5$ at convergence so this is a reasonable assumption). Define the new approximation to (4.3)–(4.4) as

$$u_{\theta N} = \left[\sum_{n=1}^{N_z} \sum_{i=1}^{n} + \sum_{n=N_z+1}^{N_r} \sum_{i=1}^{I(n)} \right] a_{(n(n-1)/2+i-1)} \Lambda_{n-i+1}(x)\, \Pi_i(z), \tag{4.11}$$

$$\varphi_N = \left[\sum_{n=1}^{N_z} \sum_{i=1}^{n} + \sum_{n=N_z+1}^{N_r} \sum_{i=1}^{I(n)} \right] b_{(n(n-1)/2+i-1)} \Psi_{n-i+1}(x)\, \Phi_i(z), \tag{4.12}$$

where $I(n)$ is an integer function of N_r, N_z, and N_i with the following properties:

$$I(n+1) \leqslant I(n), \quad I(N_z+1) = N_z - 1, \quad I(N_r) = N_i, \quad \text{if } N_i = N_r \text{ then } I(n) = n.$$

Also note that if $N_i = N_r$ this method reduces to the standard Galerkin scheme. The significance of N_r, N_z, N_i and I is best represented pictorially in figure 2. The convergence of this method relies on the absolute convergence of the series (4.3)–(4.4), allowing the terms to be summed in any order. The absolute convergence is guaranteed by the fact that u_θ is at least C^1 continuous, and φ is at least C^2 continuous (see Canuto *et al.* 1987).

4.2.1. *Convergence characteristics – a model problem*

To determine whether this method of term selection improves the rate of convergence for this type of problem we re-examine the linear stability of the Oldroyd-B fluid discussed in Avagliano & Phan-Thien (1996), for which the standard Galerkin scheme has already provided critical Deborah numbers for linear instability ($De_c = 1.661$ at $\varepsilon = 0.1$ and $\beta = 0.41$ to four significant figures). This is equivalent to the current problem with $\mu = 0$. To demonstrate that a larger number of Chebyshev modes are required we begin table 2 with $N_r = N_z = 7$ and alternately increase N_z and then N_r to 11, whilst holding N_i constant at 1. The standard Galerkin values with $N = 7$ and $N = 11$ are included.

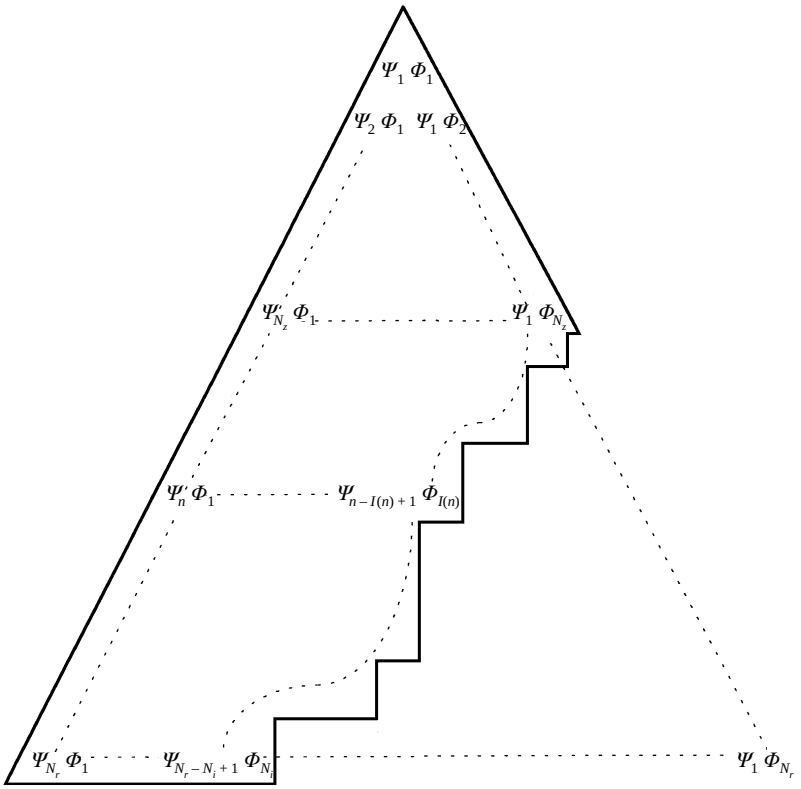

FIGURE 2. An illustration of the term selection of the alternative Galerkin scheme. The whole triangle of terms is used by the standard Galerkin scheme for $N = N_r$. The terms selected by the alternative scheme are bounded by the line.

N_r	N_z	De_c
7	7	1.8671
7	9	1.8672
7	11	1.8672
9	7	1.6973
11	7	1.6663
11	11	1.6715

TABLE 2. Convergence characteristics of an alternative Petrov–Galerkin scheme.

From the table it becomes obvious that increasing the order of approximation in the radial direction has a far greater effect on the accuracy of De_c than increasing the order in the axial direction, which has virtually no effect. The necessity of N_i for rapid convergence is illustrated in figure 3, where the accuracy of the approximation to the standard Galerkin scheme with $N = 15$ is examined. If N_i is held at 1 and N_z is increased from 7 to 15, the scheme behaves quite poorly. In fact, by $N_z = 12$ a pseudo-solution has been reached where the successive approximations agree to six significant figures, and it is only when N_z is increased to 15 that the scheme produces the correct result. However, if N_z is held constant at 8, for example, then increasing N_i from 2 up to 4 gives a solution to the standard Galerkin scheme which is accurate

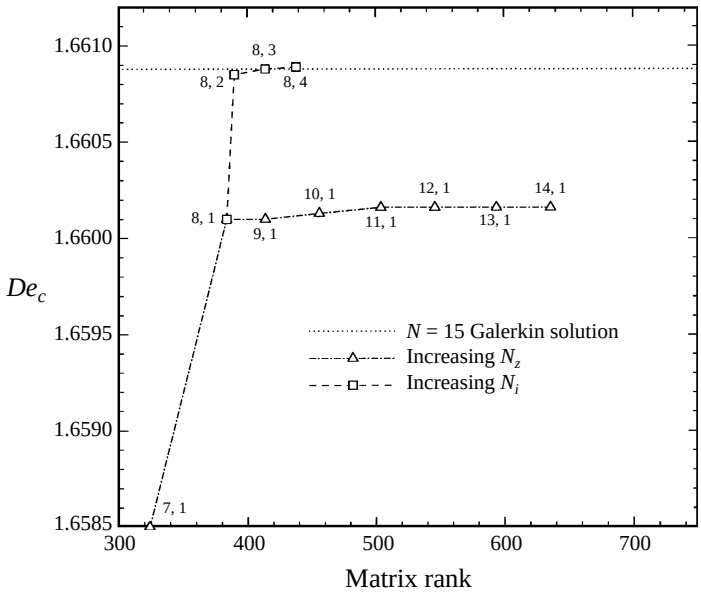

FIGURE 3. Convergence to the standard Galerkin solution with $N = N_r = 15$. The values for each approximation are labelled N_z , N_i respectively.

to six significant figures, though it only requires half the number of terms. Thus, N_i is required to introduce the modes which are of high order in the radial direction and low order in the axial direction, and also to ensure that the scheme converges to the actual solution.

4.2.2. *Convergence for* $\Psi_2 \neq 0$

The solution method is quite straightforward. With N_z and N_i held constant, N_r is increased until the increment in De_c for successive values of N_r is negligible. Once a large enough value of N_r has been reached, it is held fixed while N_i is increased. For a large enough initial choice of N_z, the solution should converge to the actual De_c. The accuracy of De_c can be verified by successively increasing N_z, N_i, and N_r by 1 and examining the new approximation. Any significant difference in the approximation to De_c would of course mean that not enough terms had been utilized initially. The method is illustrated in table 3, with $\mu = 0.025$. We found that $N_z = 8$ was more than a sufficient number of vertical modes for convergence for all aspect ratios considered and also across a wide range of Ψ_2. This phenomenon was also observed in Öztekin & Brown (1993) whose one-dimensional analysis discretized in the axial direction required as few as five trial functions for convergence of the discrete spectrum. This number increased dramatically when attempting to resolve the continuous spectrum. In Olagunju's analysis of the effect of inertia on stability of cone and plate flow (D. O. Olagunju 1996, personal communication) only four trial functions were required for the convergence of the one-dimensional model of axisymmetric secondary flow. Also, $N_i = 3$ or 4 was enough to guarantee 5 significant figures of accuracy, once N_r had been increased to a sufficiently large value.

Obtaining the final entry in table 3 requires solving for 1272 eigenvalues for each De until the critical value is determined, usually taking 5–6 iterations of a simple secant method. The standard Galerkin scheme would require solving for 4920 eigenvalues for each De. The QZ algorithm used to solve for the complex generalized eigenvalues

N_r	N_z	N_i	De_c
17	8	1	2.6370
21	8	1	2.6908
22	8	1	2.7306
25	8	1	2.7574
27	8	1	2.8256
30	8	1	2.7974
34	8	1	2.79938
35	8	1	2.79985
35	8	4	2.79981
36	8	1	2.79944
36	8	2	2.79933
36	8	3	2.79936
36	8	4	2.79936
37	8	4	2.79929
38	8	4	2.79943
39	8	4	2.79945
40	8	4	2.79945

TABLE 3. Convergence of the alternative Galerkin method.

requires $O\left(15\,(3N_T)^3\right)$ flops for each iteration (Golub & Van Loan 1983) and is $O\left((3N_T)^2\right)$ in storage, so that the equivalent standard Galerkin solution for this problem would take 64 times as long, assuming that storage space was available for the system matrices.

In essence, the eigenvalue problem being solved is identical to that given in (4.10), with the exception that 3 rows and columns are removed from the system matrices for each term excluded in the approximations (4.11)–(4.12). This procedure will infrequently lead to the production of eigenvalues with positive real part, due to catastrophic cancellation. These spurious modes are easily distinguishable and can be ignored in the solution process. This difficulty would not arise if the problem were a non-homogeneous boundary value problem rather than an eigenvalue problem.

5. Results and discussion

Phan-Thien & Huilgol (1985) conducted a theoretical analysis of the effect of Ψ_2 on torsional flow stability. The model they employed was restricted to an infinite radial domain and admitted axisymmetric disturbances of von Kármán form only. The predicted form of the disturbance was a single semi-infinite recirculation with a critical Deborah number given by

$$De_c = 2\pi/(\beta\,[2\,(6-\mu)+\beta\,(2-\mu)\,(4-3\mu)])^{1/2} \tag{5.1}$$

Their findings were consistent with, for example, Giesekus (1966) and Sun & Denn (1972) who agree that a negative Ψ_2 has a stabilizing effect on the base solution. More recent analysis by Shaqfeh, Muller & Larson (1992) for Taylor–Couette flow, in which Ψ_2 is introduced though a second-order fluid-type term, also concludes that negative Ψ_2 has a stabilizing effect on the base flow. The 4-mode Giesekus model employed by Öztekin, Brown & McKinley (1994) also incorporates a small negative Ψ_2 via the introduction of a mobility parameter. However, there is also a large amount of shear thinning in this model introduced through the same mobility parameter, so definitive

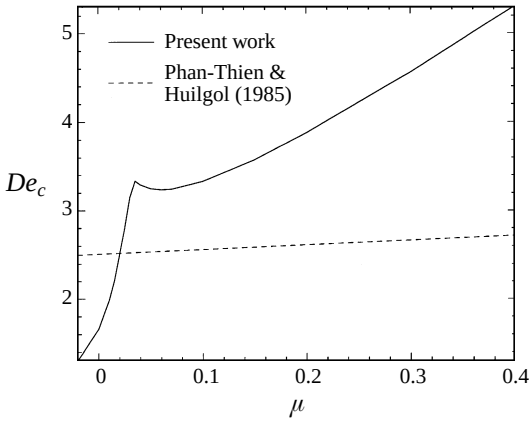

FIGURE 4. Critical Deborah number as a function of the second normal stress difference parameter μ for the current work, and also a comparison with Phan-Thien & Huilgol (1985). Here $\varepsilon = 0.1$, and $\beta = 0.41$.

evidence of the effect of Ψ_2 is not so easily obtained. It is now accepted that negative Ψ_2 stabilizes a wide variety of rotational flows (e.g. Larson 1992).

For small μ there is very little increase in De_c above that obtained for the Oldroyd-B model using the result (5.1). Experimental evidence for polyisobutylene- and polystyrene-based Boger fluids (Magda *et al.* 1991) suggest that Ψ_2 is indeed small. The combination of these results suggests that Ψ_2 can be ignored when modelling the rheology of these Boger fluids. Figure 4 illustrates the marked difference in the stability with the inclusion of a radial bounding wall and allowance for arbitrary axisymmetric disturbances.

There are clearly two regions in the neutral stability curve. A boundary layer exists in the range $-0.02 \lesssim \mu \lesssim 0.03$ where there is approximately a two-fold increase in De_c. For $\mu \gtrsim 0.03$ the gradient of the solution curve is much lower. This transition through the boundary layer has a dramatic effect upon the functional form of the secondary flow. The solution of (4.12) gives the streamlines for the disturbance flow in the form $\varphi_N = \varphi_r + \mathrm{i}\varphi_i$, where φ_r and φ_i are two real independent functions that completely determine the nature of the secondary flow. Figure 5 reveals this functional form for different values of the second normal stress difference parameter μ. For $\mu = 0$, we recover the Oldroyd-B model whose behaviour has been characterized at the onset of linear instability in Avagliano & Phan-Thien (1996), and is shown in figure 5 (*a*). Here several roll cells form near the outer edge and propagate either radially inwards or outwards within this small banded region of the domain. Choosing a value of $\mu = 0.025$, just inside the boundary layer region the solution alters to that shown in figure 5 (*b*). Here the general nature of the disturbance is the same, with the formation of roll cells whose size scales approximately with the gap width of the plates. However, the region in which the roll cells form has moved appreciably towards the centre of the discs. In the theoretical analyses conducted on stability of parallel-plate flow to date (e.g. Öztekin & Brown 1993 and Avagliano & Phan-Thien 1996 using the Oldroyd-B model, and Byars *et al.* 1994 using the Chilcott–Rallison model) the main discrepancies with experimental results have been the prediction of too low a value of De_c, and an incorrect prediction of the location of the region in which the disturbance manifests itself. The addition of a small negative Ψ_2 may then possibly alleviate both of the problems somewhat in the finite domain. At $\mu = 0.035$,

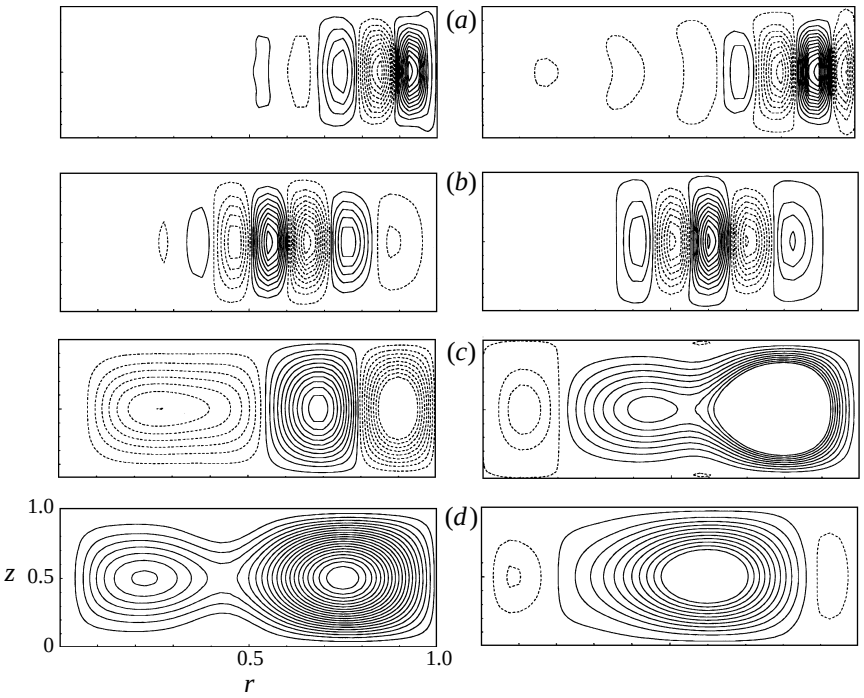

FIGURE 5. φ_r (left) and φ_i (right), for (*a*) $\mu = 0$, (*b*) $\mu = 0.025$, (*c*) $\mu = 0.035$, and (*d*) $\mu = 0.4$. All eigenvectors are determined with $\varepsilon = 0.1$ and $\beta = 0.41$.

just outside the boundary layer, the disturbance has radically altered form again (figure 5*c*). The roll cells have elongated and merged so that three of them cover the entire fluid domain and the structure is qualitatively little different to figure 5(*d*) with $\mu = 0.4$.

It is also worth mentioning the effect of negative Ψ_2 on $\mathrm{Im}(\sigma)$, which is important in determining wave speed of the disturbances. As expected, $\mathrm{Im}(\sigma)$ is also significantly altered for small μ. Using the representative example at $\beta = 0.41$ and $\varepsilon = 0.1$, we have for the Oldroyd-B model $\mathrm{Im}(\sigma) = 0.89$, whilst for $\mu = 0.025$ we have $\mathrm{Im}(\sigma) = 1.21$. This represents an increase in the predicted wave speed which, considering the experimental results of Byars *et al.* (1994), is again an improvement over the Oldroyd-B model.

The area of greatest rheological interest when examining instability of Boger fluids in torsional flow is the boundary layer region $0 < \mu \lesssim 0.03$. For the larger negative values of Ψ_2, which are a feature of more concentrated solutions of long-chain polymers in a viscous solvent, another type of instability occurs known as *edge fracture*. Here an axisymmetric indentation forms in the free surface at the plate edges reducing the effective shear area. Tanner & Keentok (1983) have shown for a second-order fluid that large negative Ψ_2 contributes to edge fracture, whilst small Ψ_2 inhibits edge fracture. A more refined analysis by Huilgol, Panizza & Payne (1993) leads to the same conclusions.

A representative value of $\mu = 0.025$ was selected to illustrate the solution properties within the boundary layer region. At the onset of linear instability, the growth rate σ has zero real part and is also found to have non-zero imaginary part. This indicates a Hopf bifurcation, where the steady base flow is altered to include a time-periodic

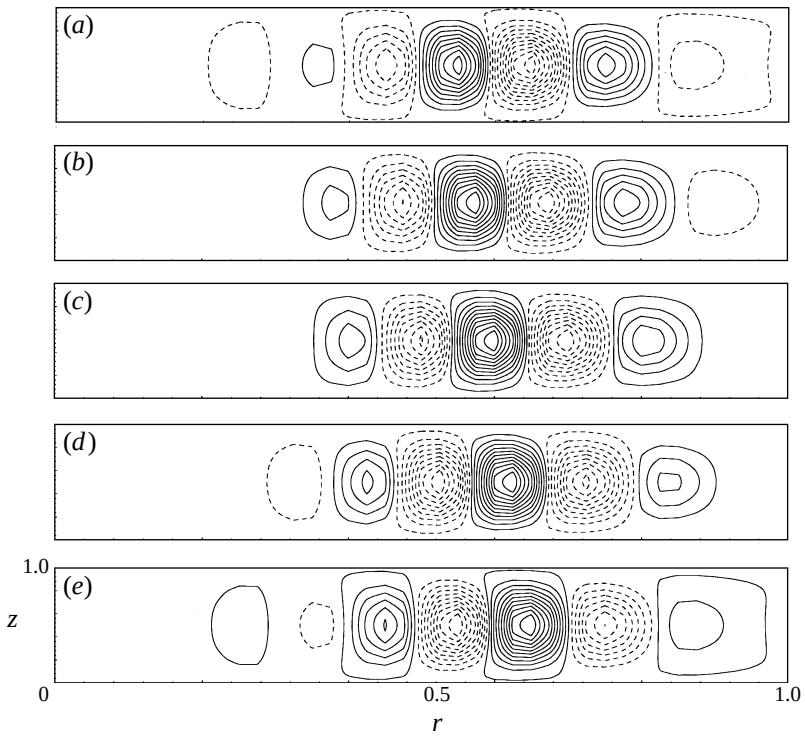

FIGURE 6. Time evolution of the first of two possible secondary flows, with roll cells travelling radially outwards. The flow is shown at times (*a*) $t = 0$, (*b*) $t = T/8$, (*c*) $t = T/4$, (*d*) $t = 3T/8$, and (*e*) $t = T/2$, where T is the period of oscillation. Here $De_c = 2.8$, $\varepsilon = 0.1$, and $\beta = 0.41$.

secondary flow. Substitution of φ_N into (3.1) reveals that two possible solutions exist for this secondary flow corresponding to the complex-conjugate critical eigenvalues obtained in (4.10). The flows are basically a set of axisymmetric roll cells which travel either radially outwards (figure 6) or inwards (figure 7).

In the two flow visualization experiments conducted examining torsional flow stability, McKinley *et al.* (1991) observed both types of secondary flow though the roll cells began at the centre and outer edge of the discs as opposed to the median radial location predicted. Byars *et al.* (1994), however, observed only axisymmetric roll cells and non-axisymmetric spirals which appeared to travel outwards.

The current model is somewhat less sensitive to changes in aspect ratio than the Oldroyd-B model (figure 8). This is due to the fact that the thickness of the boundary layer is also a function of the aspect ratio and so the stabilizing effect will be different for each geometry for the same value of μ. For example, at $\varepsilon = 0.08$, the solution structure has already changed to one of larger extended roll cells. The experimental values obtained for the onset of instability by McKinley *et al.* (1991, squares) and Byars *et al.* (1994, circles) have been included for comparison. Also included is a variant of the results of McKinley *et al.* (1991, triangles), used for experimental comparison in Öztekin & Brown (1993) and Avagliano & Phan-Thien (1996). Here the relaxation time for the Oldroyd-B model has been scaled to incorporate the shear thinning occurring at the critical rotation rate. Essentially the scaling takes into

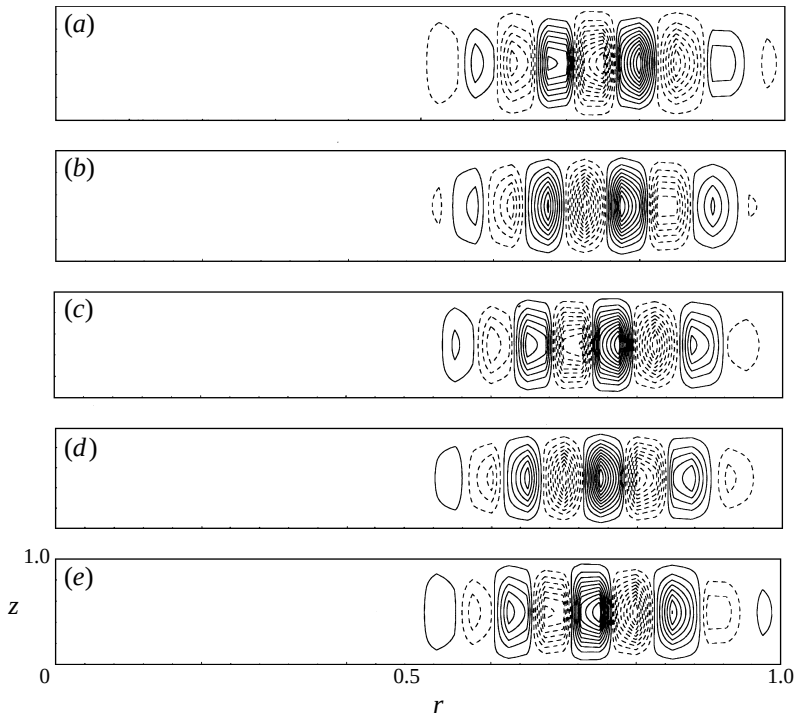

FIGURE 7. Time evolution of the second of two possible secondary flows, with roll cells travelling radially inwards. The flow is shown at times a) $t = 0$, b) $t = T/8$, c) $t = T/4$, d) $t = 3T/8$, and e) $t = T/2$, where T is the period of oscillation. Here $De_c = 2.11$, $\varepsilon = 0.05$, and $\beta = 0.41$.

account the shear thinning of Ψ_1 at higher shear rates,

$$\lambda(\dot{\gamma}) = \frac{\Psi_1(\dot{\gamma})}{2\,(\eta(\dot{\gamma}) - \eta_s)}.$$

The good agreement between the scaled experimental results of McKinley *et al.* (1991) and the Oldroyd-B model is probably fortuitous since the results of Byars *et al.* (1994) using the same Boger fluid would not scale so well. Also the functional form of the disturbance is modelled quite poorly by the Oldroyd-B model and has been improved by the inclusion of Ψ_2. Since the experimental results are still 2–3 times as large as those observed here, they only serve to illustrate that a more sophisticated multimode model which captures the shear-thinning behaviour of the Boger fluids used in these experiments as well as incorporating a small negative Ψ_2 is required to make more accurate predictions of the nature of these relatively simple viscoelastic fluids in the simplest of geometries. Such progress has already been made in a semi-infinite cone-and-plate geometry by Öztekin *et al.* (1994) using a four-mode Giesekus model to more precisely match the rheology of their Boger fluid.

We do not include the theoretical results of Öztekin & Brown (1993), and of Byars *et al.* (1994) in figure 8, since they were obtained by a linearized stability analysis on a semi-infinite domain: given De and the rheological parameters, a form of the disturbances, which involved a critical radius R^*, was postulated, and the resulting eigenvalue problem was solved for the critical radius. Both sets of results (summarized in figure 18 of Shaqfeh 1996), predict a critical value of De and the kinematics of the flow at the onset of linear instability, but are only valid for a semi-infinite radial

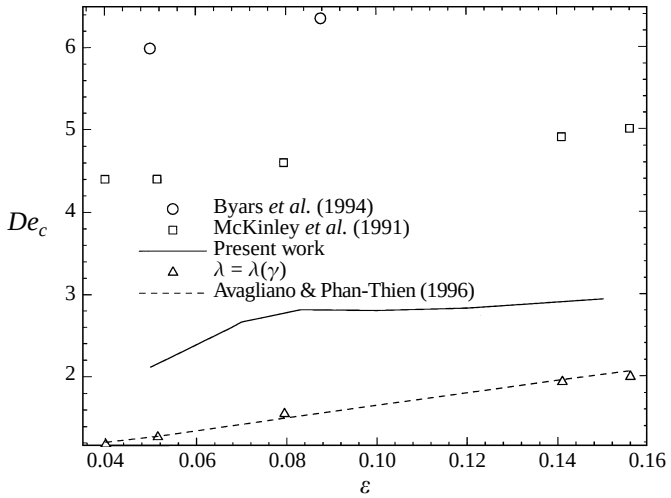

FIGURE 8. Critical Deborah number as a function of aspect ratio. $\beta = 0.41$ for all results, and $\mu = 0.025$ for the present work.

domain. The interpretation of the results for a finite domain is not clear. The difficulty is similar to that encountered when interpreting the results of Phan-Thien (1983) for the finite domain. Phan-Thien postulated the existence of axisymmetric disturbances of von Kármán form, which were shown to exist at a critical value of De. The solution cannot be generalized to the finite domain since the assumed form of the kinematics cannot satisfy boundary conditions imposed at the outer radius. As such the result serves as an indicator of the existence of instability in the finite domain, rather than a solution for this domain.

Since the domain is semi-infinite r_* must be rescaled by h, so that $r = r_*/h$. In the case of the Oldroyd-B model, Öztekin & Brown (1993) found that for a given De, the flow was unstable for all $r > R^*_{crit}$. The interpretation of these results for a finite domain seems clear. For a given experiment with dimensionless plate radius R_0, the critical value of De is determined from the neutral stability curve of R^* vs. De with $R^*_{crit} = R_0$ (Öztekin & Brown 1993; Shaqfeh 1996). However, at this critical value of De the flow instability is predicted to lie *outside* the fluid domain, so the kinematics of the solution for $r > R^*_{crit}$ give no information about the secondary flow instability that develops in a finite domain. Only the critical value of De for a finite domain is predicted with this model, though this also is not necessarily the case. Any secondary flow resulting from linear instability must satisfy imposed boundary conditions at R_0. The instability determined by Öztekin & Brown (1993) from a radially localized expansion will not necessarily satisfy these conditions.

For the Chilcott–Rallison model used in Byars *et al.* (1994) an extra parameter L determining dumbbell extensibility ($L \to \infty$ recovers the Oldroyd-B model) is employed to incorporate shear thinning. The analysis is also conducted in the semi-infinite domain. For a given value of De they also find that the flow is linearly unstable beyond a critical radius $r > R^*_1$. However, due to the effect of shear thinning of N_1 the flow restabilized at a second critical radius R^*_2 beyond which the viscometric solution was still stable. For a given value of L determined by fluid rheology the neutral stability curve of R^* vs. De now contains a turning point at some minimum value of $De = De^*$ where $R^*_1 = R^*_2 = R_{C-R}$. The solution is then examined at the

experimental value of $De_c > De^*$. The flow is already unstable at this value and the disturbances are confined between the two critical radii R_1^* and R_2^*. However, the flow surely must have gone unstable at an earlier Deborah number De^* when $R^* = R_{C-R}$. From the linearized stability analysis, De^* is the critical Deborah number predicted by the theory.

The interpretation for the finite domain is then similar to that for the Oldroyd-B model. If $R_0 > R_{C-R}$ then De^* is the predicted critical De for the flow, and this value will be greater than that predicted by the Oldroyd-B model. If $R_0 < R_{C-R}$ then the critical De is determined from the lower branch of the neutral stability curve R^* vs. De where $R^* = R_1^*$. The kinematics of the linear instability solution will still lie outside the fluid domain.

6. Mechanism behind the instability

Larson, Shaqfeh & Muller (1990) were the first to suggest that the mechanism behind instability in these viscoelastic flows with curved streamlines was due to a coupling between the disturbance velocity and base-state stress gradients leading to a perturbation in the hoop stress $\tau_{\theta\theta}$. This perturbation is then able to drive a secondary flow in a direction perpendicular to the streamlines of the base flow. Subsequent energy analyses by Joo & Shaqfeh (1992) and Byars *et al.* (1994), and also a micromechanical argument by Öztekin & Brown (1993) have confirmed that this is indeed the primary mechanism for the instability. Effects such as the introduction of shear thinning or the use of a spectrum of relaxation times only modify this mechanism.

McKinley, Pakdel & Öztekin (1996) have recently postulated a simple criterion applicable to a wide variety of geometries for determining the stability of dilute polymer solutions. It is a criterion which relies for its success upon the mechanism described above. However, the effect of Ψ_2 was not included in the above analyses.

It is not clear why a very small negative Ψ_2 influences the stability of the parallel-plate system so dramatically. Mathematically, it is obvious that equations (3.2) and (3.3) are singular in ε^2 for the Oldroyd-B model ($\mu = 0$). The introduction of a small μ affects the highest-order derivative terms in the radial direction in a similar manner to the aspect ratio ε. The relevant dimensionless coefficients are ε^2 and $\mu De^2\beta/2$. From figure 9 (*a*) we can see that $\mu De^2\beta/2\varepsilon^2 \sim O(1)$ for a large range of ε with the rather small value of $\mu = 0.025$. Essentially, small Ψ_2 is important for this model since the extra terms which are introduced scale with the terms which are singular in the aspect ratio. Hence, the wildly varying nature of the results may be a consequence of the rheology of the particular four-constant model employed.

In order to establish the physical mechanism for the effect of Ψ_2 on the stability of the base flow, some simplifying assumptions must be made. It is not possible to allow De to be arbitrarily large as was done in Öztekin & Brown (1993); however a similar effect can be achieved by expanding u_θ and φ as a regular perturbation series in β, the retardation parameter. For an expansion around $\beta = 0$ an assumption must be made about the dependence of De on β, since $De \to \infty$ in the Newtonian limit $\beta \to 0$. All available theoretical evidence (see, for example (5.1), Phan-Thien 1983, and Olagunju 1994) for these models indicates that $De \sim O(\beta^{-1/2})$ as $\beta \to 0$, though it is enough to assume this dependence and then check the perturbation solution against the full numerical solution for small values of β.

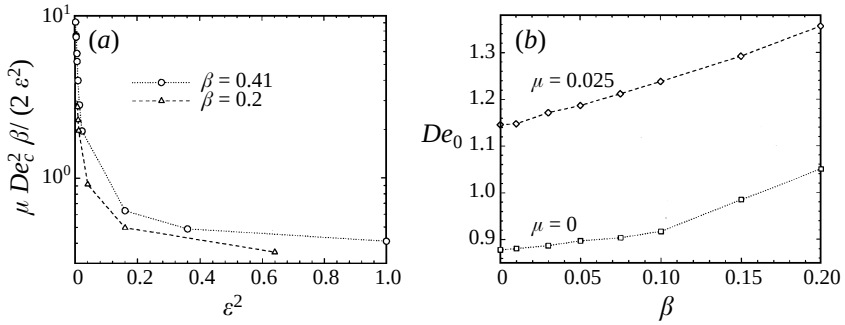

FIGURE 9. (*a*) Scaling analysis of the dimensionless coefficients of the singular terms. Note that the magnitude of $\mu De^2\beta/2$ is comparable to ε^2 for a large range of ε. (*b*) Convergence of $De_c/\beta^{1/2}$ to De_0 as β approaches zero. Both the Oldroyd-B model and the four-constant model are represented.

Expanding as

$$De = \frac{De_0}{\beta^{1/2}}, \quad u_\theta = u_{\theta 0} + \beta u_{\theta 1} + \ldots, \quad \varphi = \beta^{1/2}\left[\varphi_0 + \beta\varphi_1 + \ldots\right] \tag{6.1}$$

we find, first, for the Oldroyd-B model, that the modified stability equations of lowest order become

$$\left\{\varepsilon^2 \frac{\partial}{\partial r}\left(\frac{1}{r}\frac{\partial}{\partial r}(r u_{\theta 0})\right) + \frac{\partial^2 u_{\theta 0}}{\partial z^2}\right\} = 0, \tag{6.2}$$

$$2De_0(1+\sigma)(2+\sigma)\frac{\partial^2 u_{\theta 0}}{\partial z^2} + \underline{2De_0^2(3+\sigma)\frac{\partial^3 \varphi_0}{\partial r \partial z^2}} + (1+\sigma)^3$$
$$\times\left\{\frac{1}{r}\frac{\partial^4 \varphi_0}{\partial z^4} + 2\varepsilon^2\frac{\partial}{\partial r}\left(\frac{1}{r}\frac{\partial^3 \varphi_0}{\partial r \partial z^2}\right) + \varepsilon^4\frac{\partial}{\partial r}\left(\frac{1}{r}\frac{\partial}{\partial r}\left(r\frac{\partial}{\partial r}\left(\frac{1}{r}\frac{\partial \varphi_0}{\partial r}\right)\right)\right)\right\} = 0. \tag{6.3}$$

By uniqueness, we have $u_{\theta 0} = 0$ from (6.2). The only elastic term (the underlined term in (6.3)) is due solely to the coupling between the base-state shear stress $\tau_{\theta z}$ and azimuthal velocity v_θ and disturbance stream function φ_0. The elastic term is then convected into the radial component of the momentum equation, in agreement with the previous analyses of instability. To check that the scaling is correct for De in (6.1), the perturbation solution (represented by the circle at $\beta = 0$) is compared to the full numerical scheme (dotted lines and symbols for $\beta > 0$) in figure 9 (*b*) by plotting $De_c/\beta^{1/2} \sim De_0$ against β for various values of the retardation parameter. As expected, the full solution converges to the perturbation scheme in the limit $\beta \to 0$ for both the Oldroyd-B model and the four-constant model. This also provides an independent verification of the full numerical scheme.

The solution structure for $\mu \neq 0$ is quite different. The lowest-order terms are determined by solving the system

$$(1+\sigma)^2\left\{\varepsilon^2\frac{\partial}{\partial r}\left(\frac{1}{r}\frac{\partial}{\partial r}(r u_{\theta 0})\right) + \frac{\partial^2 u_{\theta 0}}{\partial z^2}\right\}$$
$$+\frac{\mu De_0^2}{2}\left\{\frac{\sigma}{r^2}\frac{\partial}{\partial r}\left(r^5\frac{\partial}{\partial r}\left(\frac{u_{\theta 0}}{r}\right)\right) + \frac{De_0}{r^2}\frac{\partial}{\partial r}\left(r^5\frac{\partial}{\partial r}\left(\frac{1}{r}\frac{\partial \varphi_0}{\partial r}\right)\right)\right\} = 0, \tag{6.4}$$

$$2De_0(1+\sigma)\ (2+\sigma)\frac{\partial^2 u_{\theta 0}}{\partial z^2}+2De_0^2(3+\sigma)\frac{\partial^3\varphi_0}{\partial r\partial z^2}+(1+\sigma)^3$$
$$\times\left\{\frac{1}{r}\frac{\partial^4\varphi_0}{\partial z^4}+2\varepsilon^2\frac{\partial}{\partial r}\left(\frac{1}{r}\frac{\partial^3\varphi_0}{\partial r\partial z^2}\right)+\varepsilon^4\frac{\partial}{\partial r}\left(\frac{1}{r}\frac{\partial}{\partial r}\left(r\frac{\partial}{\partial r}\left(\frac{1}{r}\frac{\partial\varphi_0}{\partial r}\right)\right)\right)\right\}$$
$$-\frac{\mu De_0}{2}\left\{(1+\sigma)^2\left[\frac{1}{r^4}\frac{\partial}{\partial r}\left(r^5\frac{\partial^2 u_{\theta 0}}{\partial z^2}\right)+\varepsilon^2\frac{\partial}{\partial r}\left(r\frac{\partial}{\partial r}\left(\frac{1}{r}\frac{\partial}{\partial r}(ru_{\theta 0})\right)\right)\right.\right.$$
$$\left.\left.-De_0\left(\varepsilon^2\frac{\partial}{\partial r}\left(r\frac{\partial}{\partial r}\left(\frac{1}{r}\frac{\partial}{\partial r}\left(r\frac{\partial\varphi_0}{\partial r}\right)\right)\right)+r^2\frac{\partial}{\partial r}\left(\frac{1}{r^3}\frac{\partial}{\partial r}\left(r^2\frac{\partial^2\varphi_0}{\partial z^2}\right)\right)\right)\right]$$
$$\left.+4De_0(1+\sigma)\left[\frac{\partial^3\varphi_0}{\partial r\partial z^2}-\frac{1}{r}\frac{\partial^2\varphi_0}{\partial z^2}\right]\right\}=0. \tag{6.5}$$

The fundamental difference between this model and the Oldroyd-B model is that a non-zero μ produces a coupling between the two equations. This coupling produces a non-trivial zeroth-order term for the disturbance azimuthal velocity, i.e. $u_{\theta 0} \neq 0$. This forces a fundamental change in the nature of the solution, since the numerical scheme shows that u_θ is of the same order of magnitude as both the vertical and radial velocities, *even for very small values of* μ. The coupling term in (6.4) is due solely to the base-state second normal stress difference, which in this case is simply $-\tau_{rr}$. This shows that the existence of a small compressive stress acting across the streamlines of the base flow is enough to significantly enhance stability.

7. Conclusions

The inclusion of a non-zero second normal stress difference has significantly increased the difficulty of obtaining numerical solutions to the stability of torsional flow of a viscoelastic fluid, even though the constitutive equations are still linear in stress. We have presented a numerical scheme which improves the convergence of a Galerkin scheme for geometries in which the differing length scales lead to stiff boundary value problems. This method is valid for a broad range of homogeneous and non-homogeneous linear boundary value problems and is not restricted to viscoelastic fluid problems.

The inclusion of a negative Ψ_2 was found to have a dramatic effect on stability within a boundary layer region, though the general trend of improving stability is in agreement with other authors. It is also possible to determine that the coupling between the momentum equations caused by the introduction of a non-zero Ψ_2 leads to a profound change in the nature of the solution: a perturbation scheme in β showed that the coupling of the stability equation produces a non-trivial zeroth-order term for the disturbance azimuthal velocity, which is due solely to the base state second normal stress difference. The stabilization relative to the Oldroyd-B model depends on the aspect ratio ε. For small aspect ratios, it is quite dramatic (De_c changes from 1.6 to 2.8 at $\varepsilon = 0.1$) while at large aspect ratios it is less significant (De_c changes from 8.1 to 8.8 at $\varepsilon = 1$).

While an improvement over the Oldroyd-B model, the current model is still inaccurate in predicting the critical rotation rate for the onset of instability, and the general location in which the instability is visible. A multimode model that also incorporates shear thinning may be necessary to improve this correlation.

The computing facility of the Sydney Distributed Computing (SyDCom) Laboratory was used in obtaining the results reported in this paper.

REFERENCES

Avagliano, A. & Phan-Thien, N. 1996 Torsional flow: elastic instability in a finite domain. *J. Fluid Mech.* **312**, 279–298.

Bird, R. B., Armstrong, R. C. & Hassager, O. 1987 *Dynamics of Polymeric Liquids. Volume 1: Fluid Mechanics,* 2nd edn. Wiley Interscience.

Byars, J. A., Öztekin, A., Brown, R. A. & McKinley, G. H. 1994 Spiral instabilities in the flow of highly elastic fluids between rotating parallel discs. *J. Fluid Mech.* **271**, 173–218.

Canuto, C., Hussaini, M. Y., Quarteroni, A. & Zang, T. A. 1987 *Spectral Methods in Fluid Dynamics.* Springer.

Giesekus, H. 1966 Zur Stabilität von Strömungen viskoelastischer Flüssigkeiten. *Rheol. Acta* **5**, 239–252.

Golub, G. H. & Van Loan, C. F. 1996 *Matrix Computations*, 3rd edn. Johns Hopkins University Press, Baltimore.

Gottleib, D. & Orszag, S. A. 1977 *Numerical Analysis of Spectral Methods: Theory and Application.* SIAM, Philadelphia.

Huilgol, R. R., Panizza, M. & Payne, L. E. 1993 On the rectilinear flow of a second-order fluid and the role of the second normal stress difference in edge fracture in rheometry. *J. Non-Newtonian Fluid Mech.* **50**, 331–348.

Joo, Y. L. & Shaqfeh, E. S. G. 1992 A purely elastic instability in Dean and Taylor-Dean flow. *Phys. Fluids* A **4**, 524–543.

Larson, R. G. 1992 Instabilities in viscoelastic flows. *Rheol. Acta* **31**, 213–263.

Larson, R. G., Shaqfeh, E. S. G. & Muller, S. J. 1990 A purely elastic instability in Taylor-Couette flow. *J. Fluid Mech.* **218**, 573–600.

McKinley, G. H., Byars, J. A., Brown, R. A. & Armstrong, R. C. 1991 Observations on the elastic instability in cone-and-plate and plate-and-plate flow of a non-Newtonian fluid. *J. Non-Newtonian Fluid Mech.* **40**, 201–229.

McKinley, G. H., Pakdel, P. & Öztekin, A. 1996 Rheological and geometric scaling of purely elastic flow instabilities. *J. Non-Newtonian Fluid Mech.* **67**, 19–47.

Magda, J. J., Lou, J., Baek, S. G. & DeVries, K. L. 1991 Second normal stress difference of a Boger fluid. *Polymer* **32**, 2000–2009.

Olagunju, D. O. 1994 Effect of free surface and inertia on viscoelastic parallel plate flow. *J. Rheol.* **38**, 151–168.

Öztekin, A. & Brown, R. A. 1993 Instability of a viscoelastic fluid between rotating parallel discs: Analysis for the Oldroyd-B fluid. *J. Fluid Mech.* **255**, 473–502.

Öztekin, A., Brown, R. A. & McKinley, G. H. 1994 Quantitative prediction of the viscoelastic instability in cone-and-plate flow of a Boger fluid using a multimode Giesekus model. *J. Non-Newtonian Fluid Mech.* **255**, 473–502.

Peyret, R. 1989 The Chebyshev Multidomain Approach to Stiff Problems in Fluid Mechanics. In *Proc. ICOSAHOM 1989 Conference: Spectral and higher order methods for Partial Differential Equations* (ed. C. Canuto & A. Quarterioni).

Phan-Thien, N. 1983 Coaxial-disc flow of an Oldroyd-B fluid: Exact solution and stability. *J. Non-Newtonian Fluid Mech.* **13**, 325–340.

Phan-Thien, N. & Huilgol, R. R. 1985 On the stability of the torsional flow of a class of Oldroyd-type fluid. *Rheol. Acta* **24**, 551–555.

Quinzani, L. M., McKinley, G. H., Brown, R. A. & Armstrong, R. C. 1990 Modelling the rheology of polyisobutylene solutions. *J. Rheol.* **34**, 705–748.

Shaqfeh, E. S. G. 1996 Purely elastic instabilities in viscometric flows. *Ann. Rev. Fluid Mech.* **28**, 129–185.

Shaqfeh, E. S. G., Muller, S. J. & Larson, R. G. 1992 The effects of gap width and dilute solutions properties on the viscoelastic instability. *J. Fluid Mech.* **235**, 287–317.

Sun, Z.-S. & Denn, M. M. 1972 Stability of rotational Couette flow of polymer solutions. *AIChE J.* **18**, 1010–1018.

Tanner, R. I. & Keentok, M. 1983 Shear fracture in cone-plate rheometry. *J. Rheol.* **27**, 47–57.

Zebib, A. 1984 Removal of spurious modes encountered in solving stability problems by spectral methods. *J. Comput. Phys.* **70**, 521–525.